CHIN. PHYS. LETT. Vol. 32, No. 12 (2015) 124305

Experimental Observation of Cumulative Second-Harmonic Generation of Circumferential Guided Wave Propagation in a Circular Tube *

DENG Ming-Xi(邓明晰)**, GAO Guang-Jian(高广健), LI Ming-Liang(李明亮)
Department of Physics, Logistics Engineering University, Chongqing 401331

(Received 19 September 2015)

The experimental observation of cumulative second-harmonic generation of the primary circumferential guided wave propagation is reported. A pair of wedge transducers is used to generate the primary circumferential guided wave desired and to detect its fundamental-frequency and second-harmonic amplitudes on the outside surface of the circular tube. The amplitudes of the fundamental waves and the second harmonics of the circumferential guided wave propagation are measured for different separations between the two wedge transducers. At the driving frequency where the primary and the double-frequency circumferential guided waves have the same linear phase velocities, the clear second-harmonic signals can be observed. The quantitative relationships between the second-harmonic amplitudes and circumferential angle are analyzed. It is experimentally verified that the second harmonics of primary circumferential guided waves do have a cumulative growth effect with the circumferential angle.

PACS: 43.35.+d, 43.25.+y, 43.20.Mv DOI: 10.1088/0256-307X/32/12/124305

It is well known that ultrasonic guided waves can propagate relatively long distances, and provide an effective means for nondestructive evaluation of structural components.[1] In the past twenty years, the effect of second-harmonic generation of ultrasonic guided wave propagation has attracted more and more attention for its excellent ability in accurately characterizing the changing aspects of material microstructures such as the dislocation density, precipitates, inclusions, and voids.[2–9] So far, the performed theoretical and experimental investigations of the nonlinear effect of guided wave propagation and its applications mainly focus on the cases where ultrasonic guided waves propagate in plate-like structures.[9–16] Moreover, the nonlinear effect of axial guided waves that propagate axially along the tubes has also been examined.[17,18] However, as an elementary mode of guided waves propagating along the circumference of the tubes (referred to as circumferential guided wave mode),[19] its nonlinear effect has not been investigated until recently by Gao *et al.*[20] It is theoretically found that, under some conditions, the second harmonics of the primary (fundamental) circumferential guided wave propagation may have strong nonlinearity, i.e., the second harmonics may grow in amplitude with circumferential angles. Experimental observation of the strong nonlinear effect of the primary circumferential guided wave propagation is of substantial significance for possible practical applications.[15,16] This study reports an experimental observation focused on the cumulative growth effect of second harmonics of circumferential guided wave propagation in a circular tube.

Within the second-order perturbation approximation, the nonlinear effect of circumferential guided wave propagation in a circular tube has been investigated to date.[20] The fields of the second harmonics of primary circumferential guided wave propagation are considered as superpositions of the fields of a series of double frequency circumferential guided wave (DFCGW) modes. It is theoretically found that the amplitude of the DFCGW mode can grow with circumferential angle when its linear phase velocity matches with that of the primary circumferential guided wave. The circular tube considered here is a stainless steel tube with an inside diameter R_1 of 104.5 mm and an outside diameter R_2 of 109.5 mm. Figure 1 shows the dispersion curves for the primary circumferential guided waves and the DFCGWs. It should be noted that the physical quantity of the abscissa axis is driving frequency f for the primary waves, and is half the double frequency (i.e., $2f/2$) for the DFCGW modes.[15] The linear phase and group velocities in Fig. 1 are defined by $c_{\rm P}^{(i)} = R_2\omega^{(i)}/n^{(i)}$ and $c_{\rm g}^{(i)} = R_2 d\omega^{(i)}/dn^{(i)}$ ($i = 1, 2$; $\omega^{(1)} = 2\pi f$ and $\omega^{(2)} = 4\pi f$), where the superscript (i)=(1) or (2) means the primary or DFCGW mode, respectively, and $n^{(i)}$ is the corresponding angular wave number.[19,20]

It can readily be found that the dispersion curves of the given circumferential guided wave mode and a DFCGW intersect at the driving frequency given by the vertical dashed line V. The horizontal dashed line H determines the corresponding linear phase velocity. There is second-harmonic generation in conjunction with the primary circumferential guided wave mode (denoted by point P_0 in Fig. 1) that can be selectively generated, and the corresponding fields of second harmonics can be decomposed into the fields of a series of DFCGWs.[13,20] The intersections between the dashed line V and the dispersion curves of the DFCGWs (denoted by points D_0, D_1, D_2, D_3, D_4, etc.) represent the DFCGW modes constituting the fields of second harmonics accompanying the primary circumferential guided wave (point P_0) propagation.[20] The superposition of points P_0 and D_0 means that the linear phase velocity of the primary circumferential guided wave (point P_0) equals to that of the DFCGW mode (point D_0) (i.e., $c_{\rm P}^{(1)} = c_{\rm P}^{(2)}$) at the driving frequency

*Supported by the National Natural Science Foundation of China under Grant Nos 11474361 and 11274388.
**Corresponding author. Email: dengmx65@yahoo.com
© 2015 Chinese Physical Society and IOP Publishing Ltd

given by the dashed line V. Therefore the DFCGW mode (point D_0) may have a cumulative growth effect and the contribution of the other DFCGW modes (points D_1, D_2, D_3, D_4, etc.) to the second harmonic field can be ignored.[13,20] Thus the second-harmonic signal of the circumferential guided wave (point P_0) propagation is ultimately determined by the specified DFCGW mode (point D_0). It is notable that the group velocity matching condition between the primary guided wave mode (point P_0) and the DFCGW mode (point D_0) is also satisfied (see Fig. 1(b); $c_{\rm g}^{(1)} = c_{\rm g}^{(2)} = 2.169\,{\rm km/s}$).[21,22]

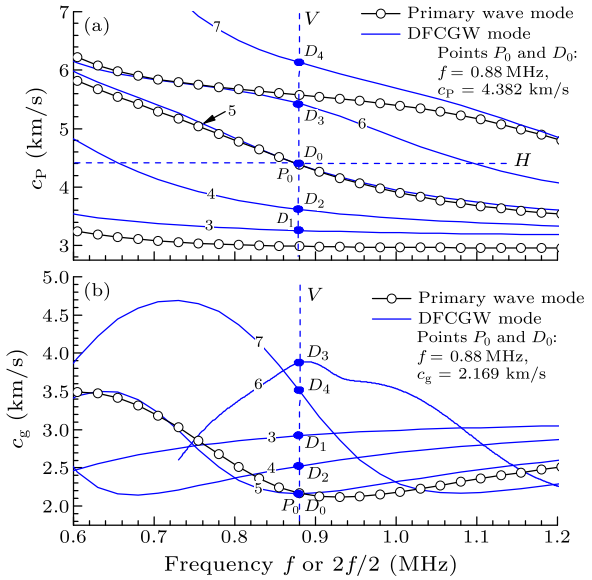

Fig. 1. (Color online) Dispersion curves for the primary circumferential guided waves and the DFCGWs in a stainless steel tube: (a) linear phase and (b) group velocities.

Figure 2 illustrates the experimental setup for the measurements of circumferential guided wave propagation. We use one wedge transducer (Tx, located on the outside surface of the stainless steel tube) to generate the circumferential guided wave mode desired (point P_0), and use another wedge transducer (Rx) to detect the corresponding primary and secondary waves. Both Tx and Rx consist of a plexiglas wedge (self-manufactured) and a longitudinal wave transducer (Model V403S or A403S, Panametrics Inc.) with an effective rectangular area of 13 mm × 25 mm. The oblique angle α of the two wedges is the same, and is determined by $\alpha = \sin^{-1}(c_{\rm L}/c_{\rm P})$, where $c_{\rm P}$ is the linear phase velocity of the circumferential guided wave (point P_0) and $c_{\rm L}$ is the longitudinal wave velocity of the wedge material (plexiglas, $c_{\rm L} = 2.717\,{\rm km/s}$). The value of $c_{\rm P}$ is determined by the dashed line H in Fig. 1(a), and it is 4.382 km/s. Thus the oblique angle α of the wedges is 38.3°. It can be expected that the refraction of the bulk longitudinal wave (generated by the longitudinal wave transducer in Tx) from the plexiglas wedge into the stainless steel tube may induce the formation of the desired guided wave mode (point P_0). Moreover, it should be pointed out that although the central frequency of the two longitudinal transducers (Models V403S and A403S, Panametrics Inc.) is around 2.25 MHz, the following experimental results have shown that there are still adequate sensitivities near the driving frequency (given by the dashed line V in Fig. 1) and its double frequency.

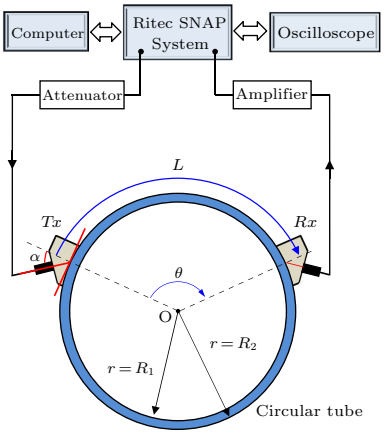

Fig. 2. (Color online) Experimental setup for measurements of circumferential guided wave propagation.

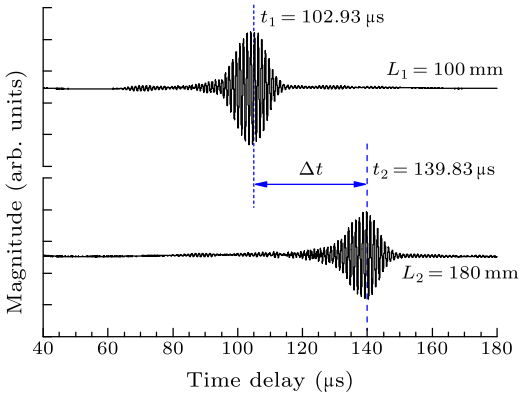

Fig. 3. Time-domain signals of the primary circumferential guided wave mode (point P_0 in Fig. 1) for arc length $L_1 = 100$ mm and $L_2 = 180$ mm.

The Ritec SNAP system (Ritec Inc.) in Fig. 2 is used to generate sinusoidal tone-burst voltages (with the carrier frequency f and the burst duration τ) that are applied to the transducer Tx, and to receive the ultrasonic signals of the primary wave and the second harmonic.[15,16,23] In the experimental examination, the transmitting transducer Tx is always driven by a 20-cycle Hanning windowed sinusoidal tone-burst voltage with the carrier frequency of 0.88 MHz (given by the vertical line V in Fig. 1; the burst duration $\tau = 20 \times 1/0.88\,\mu{\rm s}$). The spatial separation between the two transducers Tx and Rx is denoted by the arc length L or the circumferential angle θ in Fig. 2. When the transmitting transducer Tx is driven by the specified tone-burst voltage and the receiving transducer Rx is moved from one position (arc length $L_1 = 100\,{\rm mm}$) to another (arc length $L_2 = 180\,{\rm mm}$), only one clear time-domain tone-burst can be practically detected through Rx (see Fig. 3). The corresponding group velocity of the tone-burst observed is calculated to be $(L_2 - L_1)/(t_2 - t_1) = 2.168\,{\rm km/s}$, which is very close to the linear group velocity of the primary circumferential guided wave mode (point P_0) (see Fig. 1(b)). We are thus convinced that the car-

rier of the ultrasonic signal, generated by the transducer Tx and propagating along the circumference of the tube, is certainly the guided wave mode desired (point P_0).

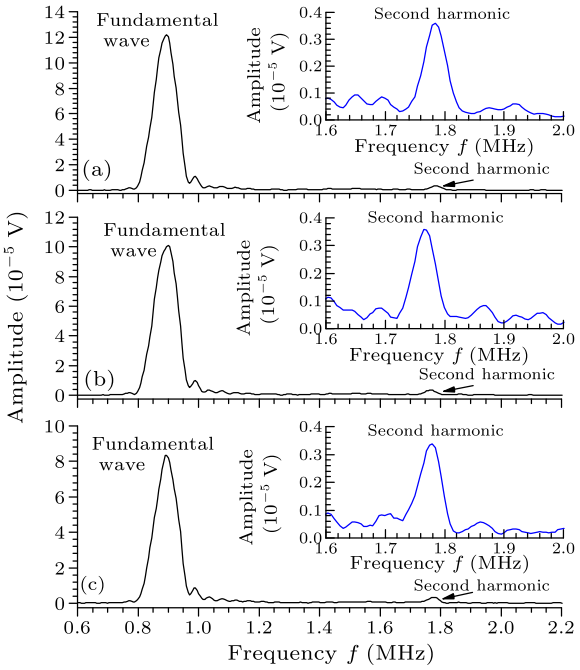

Fig. 4. (Color online) Amplitude-frequency curves of $f(t)$ for different arc lengths: (a) $L = 130$ mm, (b) $L = 170$ mm, and (c) $L = 250$ mm.

The ultrasonic time-domain tone-burst, generated by Tx and propagating along the circumference of the tube, can formally be written as $F_f(t) = A_f(t)\sin(2\pi ft + \varphi_f)$,[16,21,22] where its carrier has been experimentally verified to be the specified guided wave mode denoted by point P_0 (see Fig. 3). Here $A_f(t)$ is the modulation term, and φ_f is the corresponding phase shift in the sample. In conjunction with propagation of $F_f(t)$ along the circumference of the tube, the effect of second-harmonic generation may take place as the phase velocity matching condition is satisfied (see Fig. 1(a)). Referring to the analysis of the physical process of generation of the time-domain second harmonic by primary guided wave mode tone-burst,[21,22] it is expected that there is generation of the time-domain second harmonic by propagation of $F_f(t)$. The corresponding second-harmonic tone-burst generated can formally be given by $F_{2f}(t) = A_{2f}(t)\sin(4\pi ft + \varphi_{2f})$, where $A_{2f}(t)$ is the modulation term, and φ_{2f} is the corresponding phase shift.[16,21,22] Based on the above analysis, it can be concluded that the carrier of $F_{2f}(t)$ should be the specified DFCGW mode (denoted by point D_0 in Fig. 1). For a given arc length L in Fig. 2, the time-domain signal received by Rx (denoted by $f(t)$) should be the sum of $F_f(t)$ and $F_{2f}(t)$ in the time domain (i.e., $f(t) = F_f(t) + F_{2f}(t)$). It should be noted that, within a second-order perturbation, the magnitude of $A_{2f}(t)$ is generally far less than that of $A_f(t)$.[22] Thus, although the time-domain signal in Fig. 3 may include the second-harmonic component $F_{2f}(t)$, it can still be regarded to be $F_f(t)$ when we ascertain what the primary guided wave mode of the signal shown in Fig. 3 is.

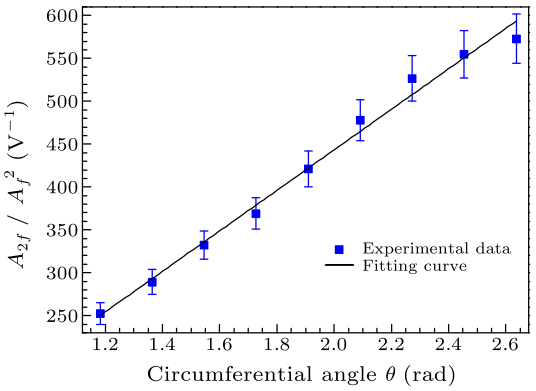

Fig. 5. (Color online) Curve of A_{2f}/A_f^2 versus circumferential angle θ at the driving frequency given by the dashed line V in Fig. 1.

Table 1. Values of A_f and A_{2f} (the averaging value of 3 times repeated measurements) as well as A_{2f}/A_f^2 versus the circumferential angle.

L (mm)	130	150	170	190	210	230	250	270	290
A_f (10^{-5} V)	12.41	10.44	10.75	10.12	7.58	8.00	8.58	7.44	7.67
A_{2f} (10^{-6} V)	3.89	3.14	3.84	3.78	2.42	3.06	3.87	3.07	3.37
A_{2f}/A_f^2 (V^{-1})	252.58	289.09	332.29	369.09	421.19	478.13	525.70	554.62	572.85
$\theta = L/R_2$ (rad)	1.19	1.37	1.55	1.74	1.92	2.10	2.28	2.47	2.65

Next we focus on observing the effect of second-harmonic generation when $F_f(t)$ propagates along the circumference of the circular tube shown in Fig. 2. We change the arc length L (or circumferential angle θ) between Tx and Rx by moving Rx along the circumference of the tube. It was varied from 130 mm to 290 mm with a moving step of 20 mm. For different arc lengths, the corresponding time-domain signals $f(t)$ like that shown in Fig. 3 are, respectively, measured and recorded by an oscilloscope (DPO 3230, Tektronix) with a sampling frequency of 1000 MHz and 10^5 sample points. Then, the digitized time-domain signal is transferred to a computer for signal processing of Fourier transform. At each receiving position of Rx, the same measurement for the corresponding time-domain signal is repeated three times; the receiving transducer Rx is completely removed and then relocated again at the same receiving position for the next repeated measurement. In the experimental measurements, the parameter setups for the experimental system are always kept unchanged.

Figure 4 shows the amplitude-frequency curves of the signal $f(t)$ detected by Rx under different arc lengths L (or circumferential angles $\theta = L/R_2$). To

save space, the amplitude-frequency curves of $f(t)$ recorded are presented only for $L = 130$ mm, 170 mm and 250 mm, respectively. Obviously, there is a clear signal of second harmonic at a fundamental frequency of 0.88 MHz for different arc lengths. Based on the amplitude-frequency curves calculated, Table 1 presents the amplitudes of the fundamental frequency and second harmonic (denoted, respectively, by A_f and A_{2f}), as well as the ratio A_{2f}/A_f^2, for different circumferential angles. Figure 5 shows the curve of A_{2f}/A_f^2 as a function of the circumferential angle θ, which clearly demonstrates the cumulative growth effect of second harmonics by primary circumferential guided wave propagation. It can thus be ensured that the clear second-harmonic signals shown in Fig. 4 should be attributed to the nonlinearity in the propagation of the ultrasonic tone-burst $F_f(t)$, whose carrier is experimentally verified to be the specified primary guided wave mode (point P_0 in Fig. 1).

In conclusion, we have clearly observed the generation of second harmonics by propagation of the primary circumferential guided wave mode. The second harmonic fields of circumferential guided waves can be decomposed into a series of DFCGWs. The DFCGW mode may have a cumulative growth effect in its amplitude when its phase velocity equals that of the primary circumferential guided wave. For different circumferential angles between the transmitting and receiving wedge transducers, the amplitudes of the primary circumferential guided waves and second harmonics on the outside surface of the circular tube have been measured at the specified driving frequency, where the primary and the double-frequency guided waves have the same linear phase velocities. The quantitative behavior of the second-harmonic amplitudes with circumferential angle has been analyzed. It is experimentally verified that, under certain conditions, the second harmonics of the primary circumferential guided wave do have a cumulative growth effect along the circumference of the circular tube.

References

[1] Rose L 2002 *J. Press. Vessel. Technol.* **124** 273
[2] Deng M X and Pei J F 2007 *Appl. Phys. Lett.* **90** 121902
[3] Bermes C, Kim J Y, Qu J M and Jacobs L J 2007 *Appl. Phys. Lett.* **90** 021901
[4] Pruell C, Kim J Y, Jacobs L J and Qu J M 2009 *Smart Mater. Struct.* **18** 035003
[5] Xiang Y X, Xuan F Z and Deng M X 2010 *Chin. Phys. Lett.* **27** 016202
[6] Xiang Y X, Deng M X, Xuan F Z, Chen H and Chen D Y 2012 *Chin. Phys. Lett.* **29** 106202
[7] Li W B, Cho Y and Achenbach J D 2012 *Smart Mater. Struct.* **21** 085019
[8] Xiang Y X, Deng M X, Liu C J and Xuan F Z 2015 *J. Appl. Phys.* **117** 214903
[9] Chillara V K and Lissenden C J 2015 *Opt. Eng.* **55** 011002
[10] Deng M X 1999 *J. Appl. Phys.* **85** 3051
[11] de Lima W J N 2000 *PhD Dissertation* (Austin: University of Texas)
[12] Deng M X 2002 *PhD Dissertation* (Shanghai: Tongji University) (in Chinese)
[13] Deng M X 2003 *J. Appl. Phys.* **94** 4152
[14] de Lima W J N and Hamilton M F 2003 *J. Sound Vib.* **265** 819
[15] Deng M X, Wang P and Lv X F 2005 *Appl. Phys. Lett.* **86** 124104
[16] Deng M X, Wang P and Lv X F 2005 *J. Phys. D: Appl. Phys.* **38** 344
[17] Chillara V K and Lissenden C J 2013 *Ultrasonics* **53** 862
[18] Liu Y, Lissenden C J and Rose J L 2014 *J. Appl. Phys.* **115** 214901
[19] Valle C, Qu J M and Jacobs L J 1999 *Int. J. Eng. Sci.* **37** 1369
[20] Gao G J, Deng M X and Li M L 2015 *Acta Phys. Sin.* **64** 184303 (in Chinese)
[21] Deng M X, Xiang Y X and Liu L B 2011 *Chin. Phys. Lett.* **28** 074301
[22] Deng M X, Xiang Y X and Liu L B 2011 *J. Appl. Phys.* **109** 113525
[23] Ritec Advanced Measurement System Model SNAP-0.25-7 Operation Manual 2000, Ritec Inc., Warwick, USA